Coherent Electronic Coupling in Atomically Thin $MoSe_2$

Akshay Singh,[1] Galan Moody,[1,*] Sanfeng Wu,[2] Yanwen Wu,[1,3] Nirmal J. Ghimire,[4,5] Jiaqiang Yan,[5,6] David G. Mandrus,[4,5,6] Xiaodong Xu,[2,7] and Xiaoqin Li[1,†]

[1]*Department of Physics, University of Texas, Austin, Texas 78712, USA*
[2]*Department of Physics, University of Washington, Seattle, Washington 98195, USA*
[3]*Department of Physics and Astronomy, University of South Carolina, Colombia, South Carolina 29208, USA*
[4]*Department of Physics and Astronomy, University of Tennessee, Knoxville, Tennessee 37996, USA*
[5]*Materials Science and Technology Division, Oak Ridge National Laboratory, Oak Ridge, Tennessee 37831, USA*
[6]*Department of Materials Science and Engineering, University of Tennessee, Knoxville, Tennessee 37996, USA*
[7]*Department of Materials Science and Engineering, University of Washington, Seattle, Washington 98195, USA*

(Received 9 January 2014; published 27 May 2014)

We report the first direct spectroscopic evidence for coherent electronic coupling between excitons and trions in atomically thin transition metal dichalcogenides, specifically monolayer $MoSe_2$. Signatures of coupling appear as isolated cross-peaks in two-color pump-probe spectra, and the line shape of the peaks reveals that the coherent coupling originates from many-body interactions. Excellent agreement between the experiment and density matrix calculations suggests that coherent exciton-trion coupling leads to the formation of a correlated state with a remarkably large binding energy.

DOI: 10.1103/PhysRevLett.112.216804 PACS numbers: 73.20.Mf, 78.47.jg, 78.67.-n

Monolayer transition metal dichalcogenides (TMDs) (e.g., MX_2, $M = \mathrm{Mo, W}$; $X = \mathrm{S, Se}$) have recently emerged as promising materials for novel electronic and photonic device applications [1]. TMDs not only represent a new class of direct band gap semiconductor materials at the two-dimensional limit [2,3], but they also exhibit intriguing coupled spin-valley physics [4–6] that enable dynamical optical control of spins and pseudospins. The fundamental optical excitation of semiconductors is an exciton—a Coulomb-bound electron-hole pair. If the Coulomb interaction is strong enough, excitons may capture an extra electron or hole, forming charged excitons known as trions.

Remarkably, the exciton and trion binding energies in monolayer TMDs are at least an order of magnitude larger than those in quasi-2D systems (e.g., GaAs quantum wells), making these quasiparticles stable at room temperature and relevant for optoelectronic devices. Such strong Coulomb interactions arise from the large carrier effective masses, strong quantum confinement, and reduced dielectric screening due to the monolayer thickness [7,8]. Previous experiments have shown that 2D excitons and trions in monolayer TMDs can be easily controlled by strain [9], doping, and an electrostatic field [8,10]. Monolayer TMDs thus provide a controllable 2D electronic system to investigate electron interaction effects such as exciton-carrier broadening [11,12], interexcitonic scattering [13], exciton valley relaxation dynamics [14], and biexciton formation [15].

An important but yet to be addressed question is whether neutral excitons and trions interact; i.e., do these quasiparticles form a coupled system? If so, are they coupled coherently? Since excitons and trions are different in both net charge and effective mass, they are expected to have different mobility and drift velocity. The existence of coupling between these two distinct quasiparticles would indicate that their response to applied electrical and optical fields cannot be treated independently. Instead, the interactions between them need to be considered in the design of efficient optoelectronic devices, including photovoltaics [16,17] and photodetectors [18]. Moreover, since these quasiparticles are localized at the corner of the first hexagonal Brillouin zone, i.e., valley excitons [4–6,10], the understanding of their interactions may shine light on the valley quantum dynamics, such as valley depolarization and decoherence.

In this Letter, we demonstrate that monolayer TMDs exhibit strong exciton-trion *coherent* coupling by performing two-color ultrafast pump-probe spectroscopy of monolayer $MoSe_2$. In a high quality sample with spectrally well-resolved exciton and trion resonances, signatures for electronic coupling between these quasiparticles are isolated as cross-peaks in a two-dimensional spectrum when the pump and probe wavelengths are tuned independently through these transitions. While incoherent population relaxation partially contributes to the coupling, density matrix calculations reveal that the unique line shape of the peaks arises from coherent exciton-trion many-body interactions, described phenomenologically as excitation induced shift and excitation induced dephasing effects.

The experimental setup is illustrated in Fig. 1(a). The output of a mode-locked Ti:sapphire laser (90 MHz repetition rate and ~15 nm FWHM bandwidth) is split into two beams. The spectrum of each beam is modified independently using a grating-based pulse shaper, producing ~1 ps pulses (~2 nm bandwidth FWHM). The pump and probe beams are combined collinearly and are focused to a ~3 μm spot on the sample. The two beams are

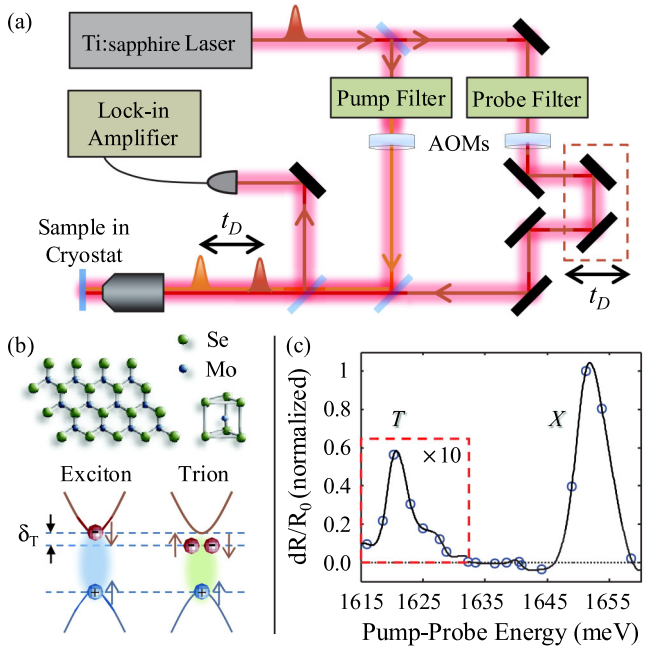

FIG. 1 (color online). (a) Schematic diagram of the two-color pump-probe setup. AOM: Acousto-Optic Modulator. (b) The hexagonal lattice structure of monolayer $MoSe_2$. Optical excitation generates either excitons (X) or trions (T) redshifted from the exciton by an energy δ_T. (c) Degenerate pump-probe spectrum (points) for delay $t_D = 0.7$ ps. The curve serves as a guide to the eye.

cross-linearly polarized to suppress scattering from the pump into the detection optics. The average power is kept below 10 μW to ensure that the signal remains in the $\chi^{(3)}$ regime, generating an estimated exciton and trion excitation density on the order of 10^{10} cm^{-2}. The pump-induced change in the probe reflectivity is recorded using a lock-in amplifier while the pump and probe wavelengths are systematically varied. Monolayer $MoSe_2$ was obtained through mechanical exfoliation onto 285-nm-thick SiO_2 on an n-doped silicon substrate. Isolation of a single layer was verified through optical and atomic force microscopy. The sample was mounted in a closed-loop cryostat and optical spectroscopy experiments were performed at 13 K to avoid phonon-mediated broadening of the resonance linewidths.

In $MoSe_2$, molybdenum and selenium atoms form a two-dimensional hexagonal lattice with a trigonal prismatic coordination [Fig. 1(b)]. At the K points in the first Brillouin zone, monolayer $MoSe_2$ has a direct band gap with similar electron and hole band curvatures [19,20]. Monolayer TMDs are unique in that broken inversion symmetry and strong spin-orbit effects couple the valley and spin degrees of freedom at the $\pm K$ points. Because cross-linear polarization is used to suppress pump scattering in the experiment, we do not distinguish between the valley or spin degrees of freedom of excitons or trions and instead focus on coherent coupling mechanisms between these quasiparticles.

We first perform a degenerate pump-probe experiment in which both beams are derived from the same pulse shaper. The degenerate pump-probe spectrum, shown in Fig. 1(c) for $t_D = 0.7$ ps, was used to identify exciton (X) and trion (T) resonances at ~1650 and ~1619 meV, respectively. The transition energies and trion binding energy of $\delta_T \approx 30$ meV are consistent with values obtained from photoluminescence spectra of similarly prepared samples [8]. One-dimensional pump-probe spectra, however, cannot provide information regarding coupling between resonances. Two-color pump-probe spectroscopy overcomes this limitation, as demonstrated by the normalized differential reflectivity spectrum shown in Fig. 2(a). The spectrum was acquired for a delay $t_D = 0.7$ ps as a compromise between avoiding ambiguities in the pump-probe time ordering and minimizing incoherent population transfer contributions. The spectrum in Fig. 2(a) features four peaks—two diagonal peaks corresponding to the exciton (X) and trion (T), respectively, a cross-peak when pumping at the exciton and probing at the trion (XT), and vice versa (TX). The appearance of cross-peaks is an unambiguous sign of exciton-trion coupling. A differential probe spectrum for resonant pumping at the exciton and trion is shown by the upper and lower horizontal slices, respectively, where the curves serve as a guide to the eye. Differences in the line shape of the XT and TX coupling peaks suggests that the coupling may not be simply due to incoherent population transfer and instead originates from exciton-trion many-body interactions.

To elucidate the coupling mechanism, we use a phenomenological model to simulate a four-level system in the excitation picture. Without making any assumption about whether exciton and trion resonances are coupled, one can map two two-level systems into a four-level system through a Hilbert space transformation, as illustrated in Fig. 2(b). State $|0\rangle$ refers to the crystal ground state in the absence of any optical excitation; states $|1\rangle$ and $|2\rangle$ represent the trion and exciton, respectively; and state $|3\rangle$ represents simultaneous excitation of the exciton and trion. The dynamics of the system, including population relaxation and dephasing, can be described by the density matrix, whose elements are related to the nonlinear signal via the optical Bloch equations [21]. We solve the optical Bloch equations perturbatively up to third order in the excitation field to calculate the nonlinear signal detected in the pump-probe experiment. The total nonlinear response can be generated using a sum-over-states expression derived from double-sided Feynman diagrams [22], illustrated in Fig. 2(c), each of which represents a quantum mechanical pathway that contributes to the signal. For each diagram, the first two arrows indicate interaction of the pump field with the sample and the third arrow is interaction of the probe field after a delay t_D. From each diagram, one can generate an expression for the perturbative evolution of the density matrix [23].

The four-level energy scheme admits the inclusion of many-body interactions in a simple and intuitive manner.

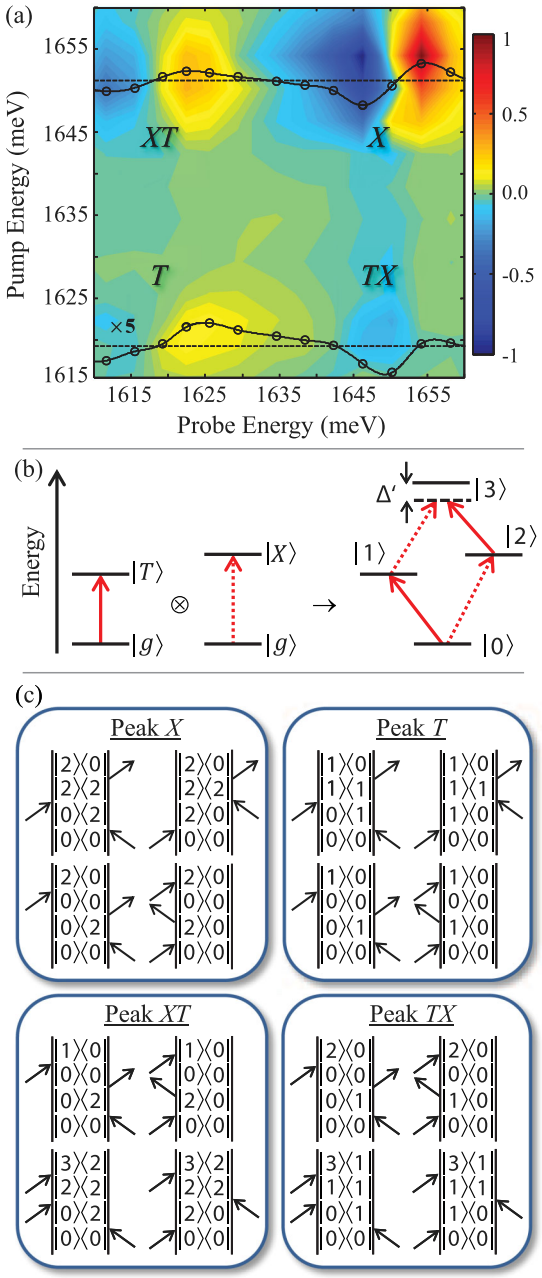

FIG. 2 (color online). (a) Normalized two-dimensional differential reflectivity spectrum featuring exciton (X) and trion (T) peaks and their coupling (XT and TX). Differential probe spectra (points) are shown for the pump resonant with the exciton (top) and trion (bottom). The curves serve as a guide to the eye. (b) Two independent two-level systems representing the exciton ($|g\rangle \rightarrow |X\rangle$) and trion (($|g\rangle \rightarrow |T\rangle$) transitions. An equivalent four-level scheme with ground ($|0\rangle$), trion ($|1\rangle$), exciton ($|2\rangle$), and exciton-trion ($|3\rangle$) states. (c) Double-sided Feynman diagrams representing the quantum pathways relevant for the experiment.

Since the lower transitions ($|0\rangle \leftrightarrow |1\rangle$ and $|0\rangle \leftrightarrow |2\rangle$) are excited by the optical field to first order in perturbation theory, while the upper transitions ($|1\rangle \leftrightarrow |3\rangle$ and $|2\rangle \leftrightarrow |3\rangle$) contribute to third order only if the lower transitions have been excited, the properties of the upper transitions dictate the interaction strength [24]. Specifically, we consider excitation-induced energy shift (EIS) and excitation-induced dephasing (EID) effects, which have been used to explain coherent exciton coupling phenomenologically in semiconductor quantum wells [25,26] and quantum dots [27,28]. EIS and EID correspond to the real and imaginary part of the renormalization energy when interaction effects are considered; thus, both effects must appear simultaneously, in principle. In the calculations, EIS effects are modeled by breaking the energy equivalence of the lower and upper transitions through a shift Δ' of state $|3\rangle$. EID effects are introduced by enhancing the dephasing rate of either or both of the upper transitions with respect to the equivalent lower transition by an amount γ'.

To illustrate how these effects are included in the calculation, we show an expression for the evolution of one density matrix component. Specifically, the quantum pathways corresponding to the bottom two Feynman diagrams for peak TX in Fig. 2(c) are described by the evolution of the third-order polarization $\rho_{13}^{(3)}$:

$$\dot{\rho}_{13}^{(3)} = \left[-i\left(\omega_{20} - \frac{\Delta'}{\hbar}\right) - (\gamma_{20} + \gamma')\right]\rho_{13}^{(3)} + \frac{i\mu_{13}}{2\hbar}\hat{E}\rho_{11}^{(2)}, \quad (1)$$

where the dipole moment, resonance energy, and dephasing rate of the transition are given by μ_{13}, $\hbar\omega_{13} \equiv \hbar\omega_{20} - \Delta'$, and $\gamma_{13} \equiv \gamma_{20} + \gamma'$, respectively, $\hat{E}$ is the electric field, and Δ' and γ' are the EIS and EID parameters for this pathway. We describe how we have chosen the parameters for all pathways in detail in the Supplemental Material [23]. However, the precise values *do not* affect the line shape qualitatively. Therefore, by carefully analyzing the line shape of each peak in the 2D map, the role of coherent many-body interactions can be identified as explained in the following. We emphasize that analyzing the entire 2D spectrum simultaneously is essential, since the line shape of each peak is sensitive to a phase shift between the reflected signal and probe. However, this phase shift is nearly constant across the entire 2D spectrum [29]; thus, the *relative* amplitude and line shape of the peaks provides critical information that enables us to distinguish between the coupling mechanisms.

To elucidate interaction effects in the measured 2D spectrum, we present and discuss results of simulated spectra in three different scenarios. First, consider the simulated spectrum in Fig. 3(a) for which no exciton-trion interactions are present. The absence of interactions is modeled by using the same parameters (dipole moment, dephasing rate, and resonance energy) for the corresponding lower and upper transitions. In this case, the quantum pathways responsible for coupling between the lower transitions are completely cancelled by pathways involving the upper transitions and no cross-peaks appear in the spectrum [30].

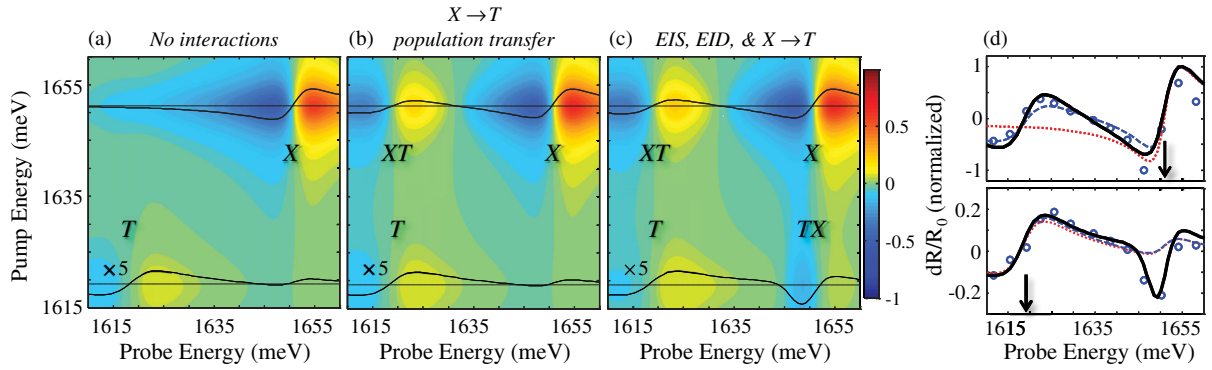

FIG. 3 (color online). Simulated two-color pump-probe spectra (a) without interactions and with interactions via (b) incoherent exciton → trion population transfer and (c) EIS, EID, and exciton → trion transfer. (d) Comparison between the experimental (points) and simulated (curves) differential probe spectrum for resonant pumping at the exciton and trion resonances (indicated by vertical arrows). The red dotted, blue dashed, and black solid curves correspond to the simulations in (a)–(c), respectively.

Secondly, in the case that only population relaxation between the exciton and trion states is considered, the 2D map [Fig. 3(b)] features highly asymmetric cross-peaks. We note that the exciton and trion relative amplitudes are related not only to quantities that characterize these transitions (dipole moments and dephasing rates), but also to the background charge density determined by the unintentional n-doping in the material [31]. Therefore, we examine the amplitude ratio between TX/T and XT/X as the key parameter for evaluating the role of incoherent population relaxation. The formation of the XT cross-peak requires the capture of an extra electron, which is energetically favorable; thus, incoherent population relaxation may lead to an appreciable amplitude of cross-peak XT in Fig. 3(b) if the background charge density is not too low. Conversely, the formation of the cross-peak TX requires additional energy from other mechanisms, such as annihilation of a phonon with an energy equal to the trion binding energy $\delta_T \approx 30$ meV. Since no significant phonon population with this energy exists at low temperature, one would expect a small amplitude ratio between TX and T. Clearly, incoherent population alone cannot explain the large amplitude of the TX peak in Fig. 2(a). Additionally, our simulation demonstrates that incoherent population transfer leads to the same line shape for TX and XT (not shown), which is inconsistent with the measured spectrum.

Finally, the role of coherent coupling mechanisms is examined. The term “coherent" is used to distinguish these mechanisms from incoherent population relaxation processes. In the simulated spectrum shown in Fig. 3(c), in which both EIS and EID are included in addition to $X \rightarrow T$ population transfer, excellent agreement with the measured spectrum is obtained. To make a more qualitative comparison between the simulated and measured spectra, two horizontal cuts are taken through the 2D maps and the results are shown in Fig. 3(d). The pump wavelength (indicated by the arrow) was tuned to the exciton and trion resonances, respectively, in the top and bottom panels. The curves are results of the simulation using a fitting procedure with a limited number of parameters (see Supplemental Material [23]). Best agreement between simulation and experiment is obtained when including EIS and EID effects (solid curves), particularly for the TX peak. This fitting suggests a binding energy for the exciton-trion correlated state of $\Delta' = 4 \pm 1.5$ meV for the excitation conditions used in the experiment [32]. We emphasize that the line shape of peak TX, namely, a negative peak rather than the dispersive line shape for the other three peaks, can only be reproduced by including the EIS effect. This distinct line shape cannot be reproduced through the inclusion or adjustment of any other parameters. These experiments demonstrate that reduced dielectric screening in TMDs results in exceptionally strong coherent coupling between quasiparticles compared to conventional semiconductors. For example, $\Delta' \approx 4$ meV observed here is at least an order of magnitude larger compared to exciton-trion coupling in a 20-nm-wide n-doped CdTe/CdMgTe quantum well [26].

Several implications stem from these results. First, in the context of valleytronics, different valley coherence and polarization dynamics were recently demonstrated for excitons and trions [10,33]. Coherent coupling between them may suggest new approaches for manipulating spin and valley degrees of freedom associated with each quasiparticle. For example, optical initialization in valley Hall experiments could be performed through the trion resonance, which exhibits a valley polarization more stable than the exciton [33]; long-lived valley polarization could be effectively transferred to the exciton intervalley coherence [10] through the coherent many-body interactions demonstrated here. Second, coherent coupling between excitons and trions lends an opportunity to drive exciton transport beyond the diffusive regime via an applied electric field [34]. In photovoltaics and detectors, coherent coupling may allow efficient exciton transport from the site of excitation to interfaces where excitons dissociate before charge collection [35]. Coherence has been demonstrated to play a key role in exciton quantum transport in photosynthesis [36–38]; similar principles may

apply for charge and energy transfer processes in TMDs. Finally, our results present a concrete example of many-body interactions in TMDs, which will facilitate the development of a full microscopic theory for their optical response. Future experiments based on advanced spectroscopic techniques such as coherent multidimensional Fourier-transform spectroscopy will provide more comprehensive information on specific quantum pathways associated with many-body interactions [39,40].

The work at UT was supported by the NSF (DMR-0747822), the Welch Foundation (F-1662), and AFOSR-PECASE: FA9550-10-1-0022. The work at UW was supported by U.S. DOE, BES, Materials Sciences and Engineering Division (DE-SC0008145). The work at ORNL was supported by U.S. DOE, Office of Basic Energy Sciences, Materials Sciences and Engineering Division.

*Present address: National Institute of Standards and Technology, Boulder, CO 80305, USA.
†elaineli@physics.utexas.edu

[1] Q. H. Wang, K. Kalantar-Zadeh, A. Kis, J. N. Coleman, and M. S. Strano, Nat. Nanotechnol. **7**, 699 (2012).
[2] K. F. Mak, C. Lee, J. Hone, J. Shan, and T. F. Heinz, Phys. Rev. Lett. **105**, 136805 (2010).
[3] A. Splendiani, L. Sun, Y. Zhang, T. Li, J. Kim, C.-Y. Chim, G. Galli, and F. Wang, Nano Lett. **10**, 1271 (2010).
[4] K. F. Mak, K. He, J. Shan, and T. F. Heinz, Nat. Nanotechnol. **7**, 494 (2012).
[5] H. Zeng, J. Dai, W. Yao, D. Xiao, and X. Cui, Nat. Nanotechnol. **7**, 490 (2012).
[6] T. Cao, G. Wang, W. Han, H. Ye, Z. Chuanrui, J. Shi, Q. Niu, P. Tan, E. Wang, B. Liu, and J. Feng, Nat. Commun. **3**, 887 (2012).
[7] K. F. Mak, K. He, C. Lee, G. H. Lee, J. Hone, T. F. Heinz, and J. Shan, Nat. Mater. **12**, 207 (2013).
[8] J. S. Ross, S. Wu, H. Yu, N. J. Ghimire, A. M. Jones, G. Aivazian, J. Yan, D. G. Mandrus, D. Xiao, W. Yao, and X. Xu, Nat. Commun. **4**, 1474 (2013).
[9] Y. Y. Hui, X. Liu, J. W., N. Y. Chan, J. Hao, Y.-T. Hsu, L.-J. Li, W. Guo, and S. P. Lau, ACS Nano **7**, 7126 (2013).
[10] A. M. Jones, H. Yu, N. J. Ghimire, S. Wu, G. Aivazian, J. S. Ross, B. Zhao, J. Yan, D. G. Mandrus, D. Xiao, W. Yao, and X. Xu, Nat. Nanotechnol. **8**, 634 (2013).
[11] R. Wang, B. A. Ruzicka, N. Kumar, M. Z. Bellus, H.-Y. Chiu, and H. Zhao, Phys. Rev. B **86**, 045406 (2012).
[12] H. Shi, R. Yan, S. Bertolazzi, J. Brivio, B. Gao, A. Kis, D. Jena, H. Xing, and L. Huang, ACS Nano **7**, 1072 (2013).
[13] S. Sim, J. Park, J.-G. Song, C. In, Y.-S. Lee, H. Kim, and H. Choi, Phys. Rev. B **88**, 075434 (2013).
[14] C. Mai, A. Barrette, Y. Yu, Y. G. Semenov, K. Wook Kim, L. Cao, and K. Gundogdu, Nano Lett. **14**, 202 (2014).
[15] E. J. Sie, Y.-H. Lee, A. J. Frenzel, J. Kong, and N. Gedik, arXiv:1312.2918.
[16] L. Britnell, R. M. Riberio, A. Eckmann, R. Jalil, B. D. Belle, A. Mishchenko, Y.-J. Kim, R. V. Gorbachev, T. Georgiou, S. V. Morozov, A. N. Grigorenko, A. K. Geim, C. Gasiraghi, A. H. Castro Neto, and K. S. Novoselov, Science **340**, 1311 (2013).
[17] M. Fontana, T. Deppe, A. K. Boyd, M. Rinzan, A. Y. Liu, M. Paranjape, and P. Barbara, Sci. Rep. **3**, 1634 (2013).
[18] O. Lopez-Sanchez, D. Lembke, M. Kayci, A. Radenovic, and A. Kis, Nat. Nanotechnol. **8**, 497 (2013).
[19] S. Tongay, J. Zhou, C. Ataca, K. Lo, T. S. Matthews, J. Li, J. C. Grossman, and J. Wu, Nano Lett. **12**, 5576 (2012).
[20] A. Ramasubramaniam, Phys. Rev. B **86**, 115409 (2012).
[21] M. O. Scully and M. S. Zubairy, *Quantum Optics*, (Cambridge University Press, Cambridge, England, 1997).
[22] S. Mukamel, *Principles of Nonlinear Optical Spectroscopy* (Oxford University Press, New York, 1995).
[23] See Supplemental Material at http://link.aps.org/supplemental/10.1103/PhysRevLett.112.216804 for details.
[24] K. Bott, O. Heller, D. Bennhardt, S. T. Cundiff, P. Thomas, E. J. Mayer, G. O. Smith, R. Eccleston, J. Kuhl, and K. Ploog, Phys. Rev. B **48**, 17418 (1993).
[25] G. Nardin, G. Moody, R. Singh, T. M. Autry, H. Li, F. Morier-Genoud, and S. T. Cundiff, Phys. Rev. Lett. **112**, 046402 (2014).
[26] G. Moody, I. A. Akimov, H. Li, R. Singh, D. R. Yakovlev, G. Karczewski, M. Wiater, T. Wojtowicz, M. Bayer, and S. T. Cundiff, Phys. Rev. Lett. **112**, 097401 (2014).
[27] J. Kasprzak, B. Patton, V. Savona, and W. Langbein, Nat. Photonics **5**, 57 (2011).
[28] G. Moody, R. Singh, H. Li, I. A. Akimov, M. Bayer, D. Reuter, A. D. Wieck, A. S. Bracker, D. Gammon, and S. T. Cundiff, Phys. Rev. B **87**, 041304 (2013).
[29] A phase shift due to the wavelength-dependent reflection coefficient is included, resulting in a change of 0.15 rad over the wavelength range of our measurement.
[30] The apparent small peak in Figs. 3(a) and 3(b) at the TX peak position is due to the spectral overlap between X and T resonances.
[31] In all mechanically exfoliated samples we have studied, the incidental doping density has been n type.
[32] The exact value of Δ' depends on the excitation density and the specific phenomenological model used. Inclusion of additional states to model exciton-exciton and trion-trion correlations reduces Δ' by approximately a factor of 2.
[33] G. Wang, L. Bouet, D. Lagarde, M. Vidal, A. Balocchi, T. Amand, X. Marie, and B. Urbaszek, arXiv:1402.6009.
[34] D. Sanvitto, F. Pulizza, A. J. Shields, P. C. M. Christianen, S. N. Holmes, M. Y. Simmons, D. A. Ritchie, J. C. Maan, and M. Pepper, Science **294**, 837 (2001).
[35] F. Meng, J. Li, S. K. Cushing, M. Zhi, and N. Wu, J. Am. Chem. Soc. **135**, 10 286 (2013).
[36] G. S. Engel, T. R. Calhoun, E. L. Read, T.-K. Ahn, T. Mancal, Y.-C. Cheng, R. E. Blankenship, and G. R. Fleming, Nature (London) **446**, 782 (2007).
[37] A. Ishizaki and G. R. Fleming, J. Phys. Chem. B **115**, 6227 (2011).
[38] E. Collini, C. Y. Wong, K. E. Wilk, P. M. G. Curmi, P. Brumer, and G. D. Scholes, Nature (London) **463**, 644 (2010).
[39] H. Li, A. D. Bristow, M. E. Siemens, G. Moody, and S. T. Cundiff, Nat. Commun. **4**, 1390 (2013).
[40] K. W. Stone, K. Gundogdu, D. B. Turner, X. Li, S. T. Cundiff, and K. A. Nelson, Science **324**, 1169 (2009).